ELSEVIER

Chemical Engineering Journal 92 (2003) 27–39

Chemical Engineering Journal

www.elsevier.com/locate/cej

Transient modelling of a HC-SCR catalyst for diesel exhaust aftertreatment

Björn Westerberg [a,b,*], Christian Künkel [c,d], C.U. Ingemar Odenbrand [c]

[a] *Department of Chemical Reaction Engineering, Chalmers University of Technology, SE-412 96 Göteborg, Sweden*
[b] *Department of Engineering, Physics and Mathematics, Mid Sweden University, SE-891 18 Örnsköldsvik, Sweden*
[c] *Department of Chemical Engineering II, Lund University, P.O. Box 124, SE-221 00 Lund, Sweden*
[d] *Scania CV AB, SE-151 87 Södertälje, Sweden*

Received 12 July 2001; accepted 11 May 2002

Abstract

The kinetics of a catalyst for hydrocarbon-selective catalytic reduction (HC-SCR) exhaust aftertreatment has been examined by means of transient experiments on a heavy-duty diesel engine rig. The influences of temperature, NO_2 concentration, and the transient injection of hydrocarbon on the conversion of NO_x, CO, and hydrocarbon were studied in a systematic manner. Hydrocarbon conversion was high and NO_x conversion was related to the amount of injected hydrocarbon at high temperatures. At lower temperatures hydrocarbon conversion was low and NO_x conversion was not directly related to hydrocarbon injection rate. Increased exhaust NO_2/NO ratio resulted in NO_x conversion at lower temperatures and also in accumulation of NO_x on the catalyst surface. The findings are in agreement with results from recent studies of the selective catalytic reduction of NO by propene. A catalyst model was designed in accordance to these studies and fitted to results from tailored and standard European transient cycles (ETC). The model shows reasonable agreement with experimental CO, NO_x and NO_2 data. Experimental hydrocarbon data are not as well reproduced, presumably due to the model approximation of hydrocarbons to one species. The full catalyst model used in the study is presented, including reaction kinetics and equations for mass and heat transfer. Mechanistic aspects are discussed and related to other studies.

Keywords: Transient modelling; Diesel exhaust; Aftertreatment; NO_x reduction; Kinetics

1. Introduction

The need for an efficient NO_x aftertreatment system for diesel exhaust is well known. The selective catalytic reduction (SCR) technique early proved to be successful [1]. It is, however, an unattractive alternative due to the need of a separate container with either ammonia or urea onboard the vehicle and an infrastructure to supply this extra chemical. Hydrocarbon-SCR (HC-SCR) instead uses the diesel fuel as reducing agent. This technique, however, increases fuel consumption and it is therefore of considerable interest that the extra amount of fuel is used as efficiently as possible.

During real use the driving conditions (engine speed and torque) vary unpredictably. As a consequence the exhaust properties (temperature, mass-flow and composition) vary irregularly. A control algorithm, i.e. a dosing strategy, is needed to continuously adjust the injection of reducing agent in accordance with prevailing conditions. The dosing strategy may be of varying complexity. In a previous study [2], a dosing strategy that determined the amount of reducing agent from the catalyst temperature and the NO_x flow was used. With this relatively simple strategy it was shown that the distribution of reducing agent during a European transient cycle (ETC) has a large impact on the total NO_x conversion. For the dosing strategy to be efficient the amount of reducing agent needs to be determined from states in the catalyst that are closely correlated to the NO_x conversion. These states can be obtained by modelling the kinetics of the catalyst in real time.

A detailed kinetic model is useful for optimisation of a dosing strategy, regardless of strategy type. A dosing strategy can certainly be optimised experimentally by an iterative procedure, based on a factorial experimental design with subsequent experiments performed in the direction of the steepest ascent. That method has been employed in another work [3]. It is, however, a time consuming procedure requiring a large number of experiments to be performed on an engine rig. Thus, costly and time-consuming laboratory work can be avoided if the optimisation is,

* Corresponding author.
E-mail address: bjorn.westerberg@mh.se (B. Westerberg).

1385-8947/02/$ – see front matter
PII: S1385-8947(02)00118-3

at least partially, performed with the aid of computer simulation.

In this work, a kinetic model is developed for a high temperature (HT) catalyst used in a HC-SCR aftertreatment system. The model is fitted to data from transient experiments performed on an engine rig. A critical part of the model is the reaction mechanism that is used. In a previous study [4], it was concluded that the NO_x reduction proceeds via the formation of a hydrocarbon intermediate and the successive reaction between this intermediate and NO_x. In this work, the model is developed further. The influences of the temperature, the NO_2 concentration and the transient injection of hydrocarbon on the conversion of NO_x, CO and hydrocarbon are studied in a systematic manner. Mechanistic aspects are discussed and related to studies of other catalysts.

2. Methods

2.1. Engine, fuel, catalysts and injection

All experiments were performed on a 6.7 l Volvo TD73 EA heavy-duty diesel engine placed in a rig capable of performing transient cycles. Swedish MK1, a commercial low-sulphur fuel (approximately 5 ppm S), was used both as engine fuel and as reducing agent. Monolithic catalytic converters supplied by Johnson Matthey were connected to the exhaust pipe. Two types of catalysts with different functions were used, a HT and a low temperature (LT) catalyst. The HT catalyst shows a substantial NO_x to N_2 conversion above 370 °C and some NO_x conversion below this temperature. The HT catalyst also shows a high, but not complete, conversion of hydrocarbon and CO above 370 °C, but a low conversion of NO to NO_2. The LT catalyst shows an almost complete conversion of hydrocarbon and CO above 200 °C. The LT catalyst also converts NO to NO_2 and shows some NO_x to N_2 and N_2O conversion around 250 °C. The volume of each catalyst brick was 6 l (diameter 229 mm, 62 channels per cm^2). A total catalyst volume of 24 l was used. The catalytic converters were insulated in order to provide adiabatic conditions. The injector consisted of an air-assisted spray nozzle, the diesel fuel being pulsed with a Bosch L-Jetronic solenoid valve. The transient response from the injector was levelled when the injected fuel was mixed with the exhaust gas. This was taken into account by applying an exponential filter with a time constant of 7.2 s, determined from a separate experiment.

2.2. Analysis of the exhaust gas

Exhaust gas was sampled upstream the first HT catalyst and downstream the first and the second HT catalyst downstream the injector (Fig. 1). The sampled gas was conducted through heated PTFE pipes to a J.U.M. Engineering model 222 heated gas pre-filter. The hydrocarbon content was determined using a J.U.M. Engineering model VE5 FID instrument. A Tecan CLD 700 EL ht chemiluminescense instrument was used for NO and $NO + NO_2$ analysis, and a Siemens Ultramat 22P for CO analysis. The CO detector had an upper detection limit of 300 ppm. N_2O was analysed with a Siemens Ultramat 5E. Water in the gas for CO and N_2O analysis was condensed using a Siemens 7 MB gas cooler. The temperature was measured with type K thermocouples at the same locations as where the exhaust gas was sampled. The mass-flow was measured with a hot wire anemometer and the engine fuel consumption was measured with a scale. The oxygen and water concentrations were determined from a mass balance and the CO and N_2O concentrations were recalculated to a wet flow.

2.3. Test procedures

Two different catalyst configurations were used, either with a HT or a LT catalyst upstream of the injector (Fig. 1). The HT configuration served as a reference, whereas the LT configuration provided a higher NO_2 content in the gas flow upstream the studied HT catalyst.

An ETC with no injection was performed with the LT configuration. This test was used to validate the thermal part of the catalyst model.

Two other types of transient tests were performed. Both tests began with a 10 min long preconditioning period (not shown in figures). The engine was first run 6 min at high speed and load to produce a large mass-flow and a high temperature, then 4 min at medium speed, but still at high load to increase the temperature further. The purpose was to obtain

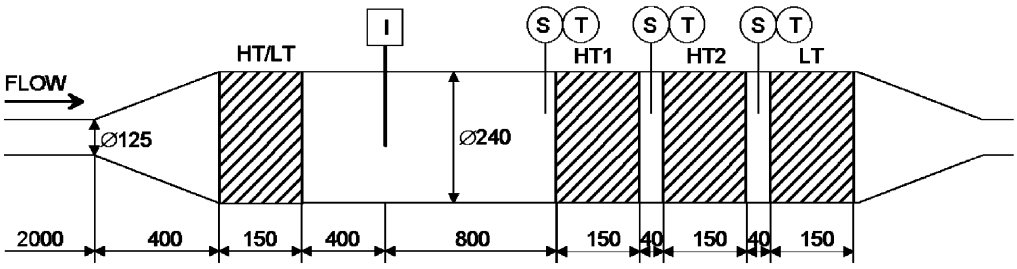

Fig. 1. Catalyst configurations during the tests. In the HT and the LT configuration the catalyst upstream the injector was a HT or a LT catalyst, respectively. I, S and T denote injector, gas sampling point and thermocouple, respectively. All measures are in mm.

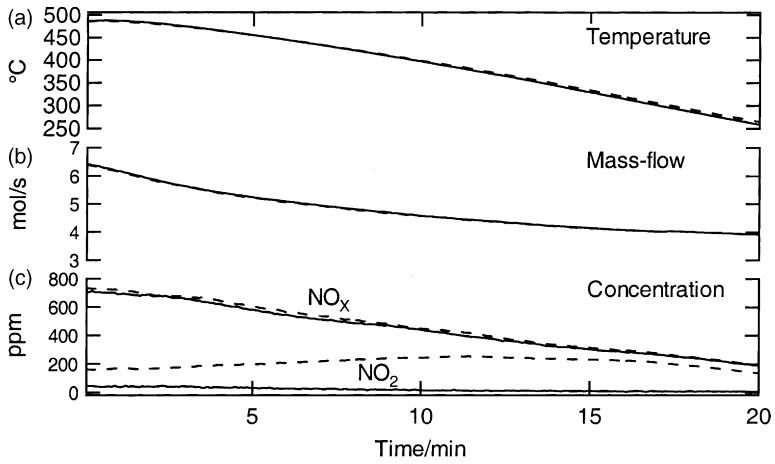

Fig. 2. (a) Temperature, (b) mass-flow and (c) NO_x and NO_2 concentration during the temperature ramp with the HT (solid) and the LT (dashed) configuration.

reproducible starting conditions between repeated tests. The high mass-flow caused the temperature to level out through the catalyst at a temperature independent of the temperature before the test. The high temperature caused the removal of accumulated species (with possibly the exception of oxygen) on the catalyst and provided a well-defined state of the catalyst.

In the first type of test, the temperature was ramped from 485 to 260 °C during 20 min, by ramping the engine load at a constant speed. Every 2 min a 30 s pulse of hydrocarbons was introduced by injecting diesel fuel. Each odd pulse was 400 ppm (C_1-units) while each even pulse was 800 ppm. This test is referred to as the temperature ramp. The temperature ramp was performed with both the LT and the HT configuration, with the purpose to obtain qualitative information about the temperature dependence of the reactions on the catalyst and the influence of an increased NO_2 concentration. In Fig. 2, the temperature, the mass-flow and the concentrations of NO_x and NO_2 upstream the first HT catalyst during the temperature ramp with the HT and the LT configuration are shown.

In the second type of test, the temperature was ramped down and up three times at three different engine speeds in order to produce different combinations of temperature, mass-flow, and NO_x concentration. Every 2 min a 30 s pulse of hydrocarbons was introduced. Each odd pulse was 750 ppm (C_1-units) while each even pulse was 1500 ppm. This test is referred to as the transient test. The transient test was only performed with the LT configuration, and the purpose was to provide experimental data for fitting the kinetic model. The test contains 48 hydrocarbon transients. This large number of transients was selected in order to force the catalyst into a permanent unsteady state, thereby providing a larger variance in the experimental data. The test both starts and ends at a high temperature. The reason for starting the test at a high temperature has already been mentioned. The reason for ending the test at a high temperature was to avoid having an unknown accumulation of

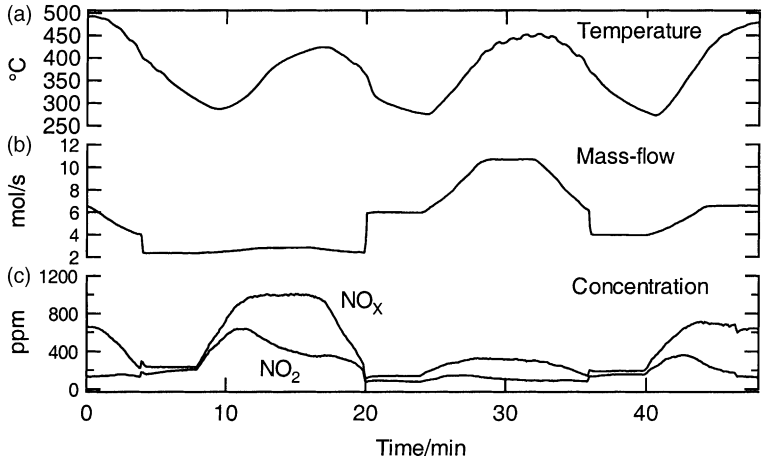

Fig. 3. (a) Temperature, (b) mass-flow and (c) NO_x and NO_2 concentration during the transient test (performed with the LT configuration only).

species on the catalyst at the end of the test. In Fig. 3, the temperature, the mass-flow and the concentrations of NO_x and NO_2 upstream the first HT catalyst during the transient test are shown. At high temperatures partial combustion of injected hydrocarbons occur upstream of the catalysts, presumably homogeneous as reported by Kharas et al. [5], resulting in a temperature increase during injection. The phenomenon is evident particularly between 28 and 36 min, when a high total mass-flow induces large hydrocarbon injections. The extent of this combustion was estimated from the temperature increase and the inlet hydrocarbon concentration used in the model was corrected accordingly.

2.4. Catalyst model

The monolithic catalyst was modelled as a series of 10 continuously stirred tanks. The number, although low with respect to the space velocity (83 000–510 000 h^{-1}), was chosen as a compromise between computational time and accuracy. For actual flow conditions a more correct number of tanks would have been between 40 and 140 [6–8]. For a first order reaction, the use of 10 tanks thus yields a relative error of less than 3% conversion. The equations for mass and energy balances have similar appearance as in a previous work [4]. The model assumes a uniform radial flow distribution, no radial temperature and concentration gradients, no axial diffusion or heat conduction, no gas phase accumulation and no diffusion resistance in the washcoat. For each tank the gas mass balance is given by

$$F_{i,k-1} - F_{i,k} - k_{c,i,k} A_k (c_{g,i,k} - c_{s,i,k}) = 0 \quad (1)$$

where $F_{i,k}$ is the molar flow of component i in tank k, $k_{c,i,k}$ is the mass transfer coefficient of component i in tank k, A_k is the wall area in tank k, $c_{g,i,k}$ and $c_{s,i,k}$ are the concentrations of component i in tank k in the gas bulk and at the catalyst surface, respectively. The surface mass balances are given by the equations

$$k_{c,i,k} A_k (c_{g,i,k} - c_{s,i,k}) = \sum_j \nu_{i,j} r_{j,k} m_{wc,k} \quad (2)$$

$$N_{cat} \frac{\partial \theta_{i,k}}{\partial t} = \sum_j \nu_{i,j} r_{j,k} \quad (3)$$

where $\nu_{i,j}$ is the stoichiometric coefficient for component i in reaction j, $r_{j,k}$ is the rate of reaction j in tank k, $m_{wc,k}$ is the mass of washcoat (active catalyst) in tank k, N_{cat} is the number of active sites per kilogram catalyst, $\theta_{i,k}$ is the coverage of surface species i in tank k and t is the time. The gas energy balance is given by

$$\sum_i (F_{i,k-1} c_{p,i} T_{g,k-1} - F_{i,k} c_{p,i} T_{g,k}) - h_k A_k (T_{g,k} - T_{s,k}) = 0 \quad (4)$$

where $c_{p,i}$ is the heat capacity for component i, h_k is the heat transfer coefficient in tank k, $T_{g,k}$ and $T_{s,k}$ are the temperatures in tank k in the gas bulk and of the catalyst, respectively. The solid energy balance is given by

$$m_{s,k} c_{p,s} \frac{\partial T_{s,k}}{\partial t} = h_k A_k (T_{g,k} - T_{s,k}) + \sum_j r_{j,k} m_{wc,k} (-\Delta H_j) \quad (5)$$

where $m_{s,k}$ is the total mass of solid material in tank k, $c_{p,s}$ is the heat capacity of the solid material and $-\Delta H_j$ is the heat of reaction j. The mass and heat transfer was described with the film model and the following expressions were used for the Sherwood and the Nusselt number [9]

$$Sh = Sh_\infty + 6.874(1000 z_m)^{-0.488} e^{-57.2 z_m} \quad (6)$$

$$Nu = Nu_\infty + 6.874(1000 z_h)^{-0.488} e^{-57.2 z_h} \quad (7)$$

where Sh_∞ and Nu_∞ are the asymptotic Sherwood and Nusselt number, respectively. For a square channel the value for Sh_∞ has been determined to be 3.087 for constant mass flux and 2.977 for constant wall concentration [9]. For Nu_∞, the value has been determined to 3.091 for constant heat flux and 2.976 for constant wall temperature [9]. In this work, 3.0 was used for both Sh_∞ and Nu_∞. The dimensionless axial distances z_m and z_h, for mass and heat transfer, respectively, are given by the equations

$$z_m = \frac{z}{d\, Re\, Sc} \quad (8)$$

$$z_h = \frac{z}{d\, Re\, Pr} \quad (9)$$

where z is the distance from the entrance, d the channel width, Re, Sc and Pr are the Reynolds, the Schmidt and the Prandtl numbers, respectively. Binary diffusion coefficients were calculated from an equation given by Fuller et al. and multicomponent diffusion coefficients were then calculated from Blanc's law [10]. Gas heat conductivities were taken from Reid [10]. Heat capacities for the gas and the monolith were taken from Barin [11]. For the diffusion coefficients, the gas heat capacity and the gas heat conductivity the average exhaust composition (77% N_2, 14% O_2, 4.4% H_2O and 4.4% CO_2) for an ETC was used. For the gas heat capacity the average temperature (350 °C) for an ETC was used.

The kinetics was described with a mean field model containing both Langmuir–Hinshelwood and Eley–Rideal type reactions. The Arrhenius expression was used for the rate constant. For adsorption the pre-exponential factor was calculated from kinetic gas theory [12,13]

$$A_{ads} = \frac{N_A RT}{\sqrt{2\pi MRT}} A N_{cat} S_0 \quad (m^3/s\,kg\,catalyst) \quad (10)$$

where N_A is the Avogadro number, M the molar mass in kg/mol, A the area of a site (assumed as 6.8×10^{-20} m^2 [14]), N_{cat} the number of active sites per kilogram catalyst and S_0 the sticking coefficient at zero coverage. S_0 was arbitrarily chosen as 0.1 and the pre-exponential factor was calculated at 350 °C (the temperature dependence neglected).

For Eley–Rideal reactions the same pre-exponential factor was used as for adsorption [12,13]. Depending on the mobility of the adsorbed species the pre-exponential factors for desorption and Langmuir–Hinshelwood reactions may vary some orders of magnitude around $10^{13}\,s^{-1}$ [12,13]. In order to minimise the number of free parameters in the model the pre-exponential factors for these kinds of reactions were set to $10^{13}\,s^{-1}$. The pre-exponential factor for oxygen adsorption was determined from thermodynamical data for the NO/NO_2 equilibrium in order to obtain a consistent entropy balance. Analogously the activation energy for oxygen desorption was determined from thermodynamical data in order to obtain a consistent enthalpy balance.

2.5. Model fitting

The kinetic model parameters (activation energies and the number of active sites) were fitted to five different sets of experimental data. Two sets of data were used from the temperature ramp with the HT configuration. In the first set the inlet conditions were taken upstream the first HT catalyst and fitting was made to the concentrations downstream the first HT catalyst. In the second set the inlet conditions were taken downstream the first HT catalyst and fitting was made to the concentrations downstream the second HT catalyst. Two similar sets of data were used from the temperature ramp with the LT configuration. Finally, one set of data was used from the transient test. In this case, the inlet conditions were taken upstream the first HT catalyst and fitting was made to the concentrations downstream the first HT catalyst. The concentrations for hydrocarbon, CO, NO, NO_2 and NO_x were weighted differently in order to yield equal sum of squares.

3. Results

In the following text, the experimental results from the temperature ramp with the HT and the LT configuration are presented. These experiments were also used to validate the kinetic model. Thus, also the results from the model are shown. The kinetic model and the justification of inferring different reaction steps are presented in the discussion.

In Fig. 4, the observed and the modelled hydrocarbon concentrations (in C_1-units) downstream the second HT catalyst during the temperature ramp with the HT configuration are shown. Also shown are temperature and hydrocarbon concentration at the inlet to the first HT catalyst (injected hydrocarbon excluded). Above 370 °C hydrocarbon conversion is 80% or higher, but below this temperature hydrocarbon conversion is less than 25%. Notable is that the conversion is somewhat lower for the first two transients than for the following four, even though the temperature is higher for the former.

In Fig. 5, the observed and the modelled hydrocarbon concentrations downstream the second HT catalyst during the temperature ramp with the LT configuration are shown. Also shown are the temperature and the hydrocarbon concentration at the inlet to the first HT catalyst (injected hydrocarbon excluded). Hydrocarbon conversion is somewhat higher compared to the experiment with the HT configuration; 85% or higher when the temperature is higher than 370 °C and less than 50% when the temperature is lower. Also in this case, hydrocarbon conversion is somewhat lower for the first two transients than for the following four.

In Fig. 6, the observed and the modelled CO concentrations downstream the second HT catalyst during the temperature ramp with the HT configuration are shown. Also shown are the temperature and the CO concentration at the inlet to

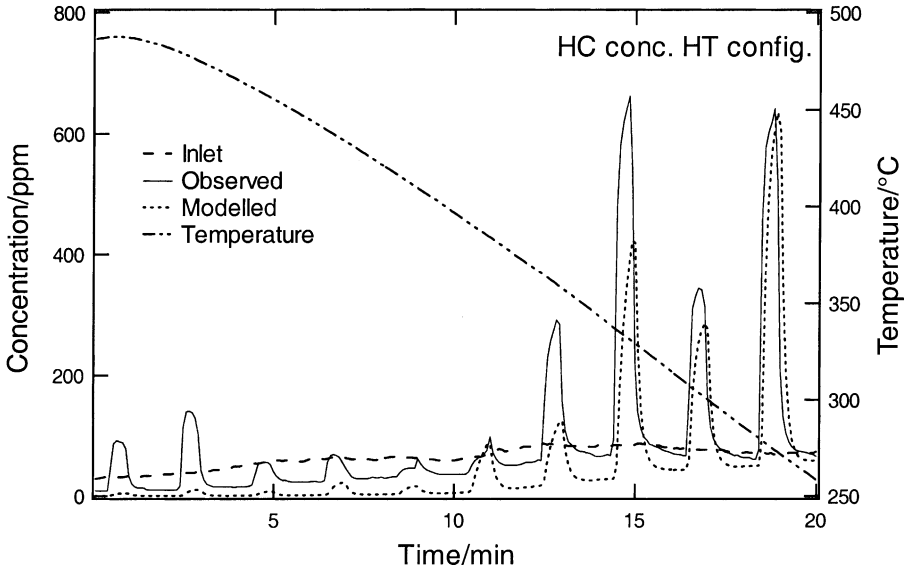

Fig. 4. Observed and modelled hydrocarbon concentrations (in C_1-units) downstream the second HT catalyst during the temperature ramp with the HT configuration. Also shown are the temperature and the hydrocarbon concentration at the inlet to the first HT catalyst (injected hydrocarbon excluded).

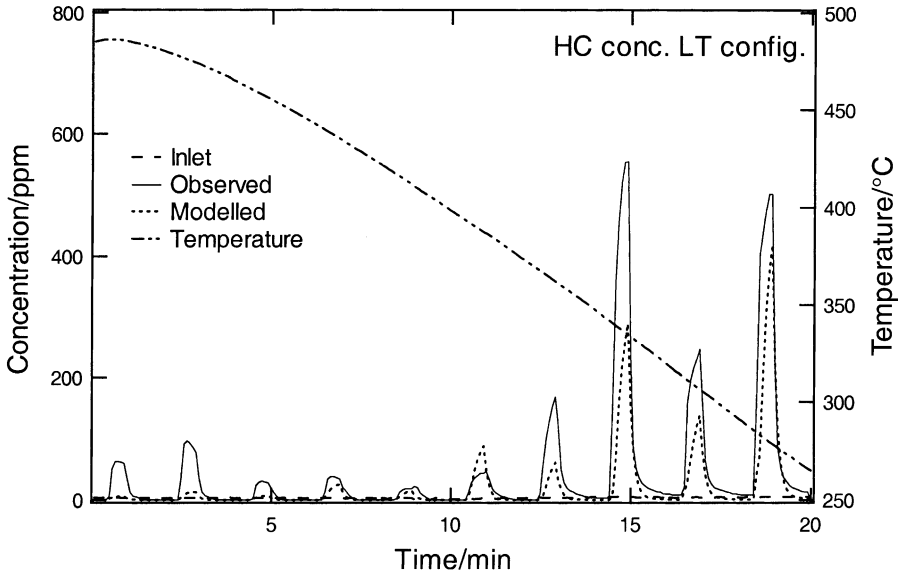

Fig. 5. Observed and modelled hydrocarbon concentrations (in C_1-units) downstream the second HT catalyst during the temperature ramp with the LT configuration. Also shown are the temperature and the hydrocarbon concentration at the inlet to the first HT catalyst (injected hydrocarbon excluded).

the first HT catalyst. During the transients CO is formed. The highest CO concentration is observed during the transient at 390 °C. Above this temperature lower CO concentrations are observed, probably due to a higher rate for further conversion to CO_2. For the transients below 390 °C less CO is formed and the response is slower and more sustained.

In Fig. 7, the observed and the modelled CO concentrations downstream the second HT catalyst during the temperature ramp with the LT configuration are shown. Also shown are the temperature and the CO concentration at the inlet to the first HT catalyst. The result is similar to that obtained with the HT configuration, but the CO concentrations during the transients above 370 °C are lower than those obtained with the HT configuration. Also in this case the highest CO concentration is observed during the transient at 390 °C and the CO concentrations observed above this temperature are lower. The formation of CO during the transients below 390 °C is of comparable size to that obtained with the HT configuration and a slower and more sustained response is observed also here.

In Fig. 8, the observed and the modelled NO_x and NO_2 concentrations downstream the second HT catalyst during the temperature ramp with the HT configuration are shown. Also shown are the temperature and the NO_x and NO_2

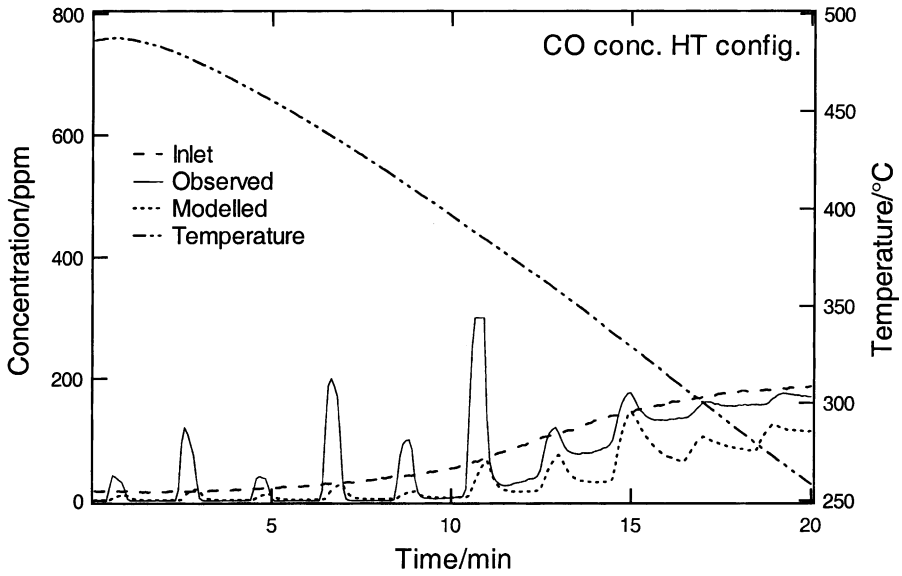

Fig. 6. Observed and modelled CO concentrations downstream the second HT catalyst during the temperature ramp with the HT configuration. Also shown are the temperature and the CO concentration at the inlet to the first HT catalyst.

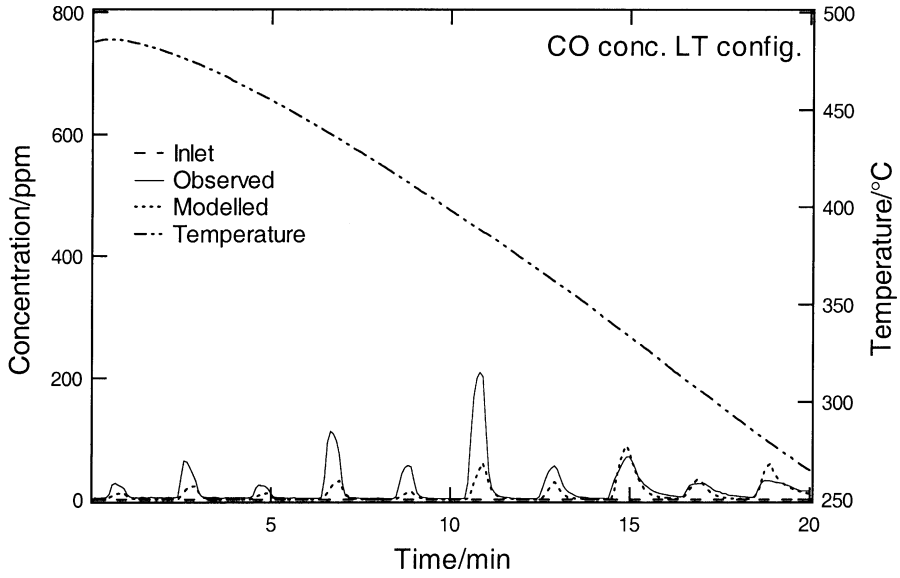

Fig. 7. Observed and modelled CO concentrations downstream the second HT catalyst during the temperature ramp with the LT configuration. Also shown are the temperature and the CO concentration at the inlet to the first HT catalyst.

concentrations at the inlet to the first HT catalyst. At temperatures above 370 °C there is a NO_x conversion related to the size of the hydrocarbon transient. Well above 370 °C the response is fast but for the two transients just above 370 °C the response is somewhat slower and more sustained. For the two transients just below 370 °C there is a small NO_x conversion but below 320 °C no NO_x conversion is observed. Above 370 °C the NO_2 concentration drops considerably during the transients and between the transients there is a small production of NO_2. Below 370 °C both the inlet and the outlet NO_2 concentrations are close to zero.

In Fig. 9, the observed and the modelled NO_x and NO_2 concentrations downstream the second HT catalyst during the temperature ramp with the LT configuration are shown. Also shown are the temperature and the NO_x and NO_2 concentrations at the inlet to the first HT catalyst. As for the HT configuration there is a NO_x conversion related to the size of the hydrocarbon transient at temperatures above 370 °C. For the two transients just above 370 °C there is a short NO_x desorption peak in the beginning of the transient. The height of this peak grows as the temperature decreases until the second transient below 370 °C. Then the height decreases

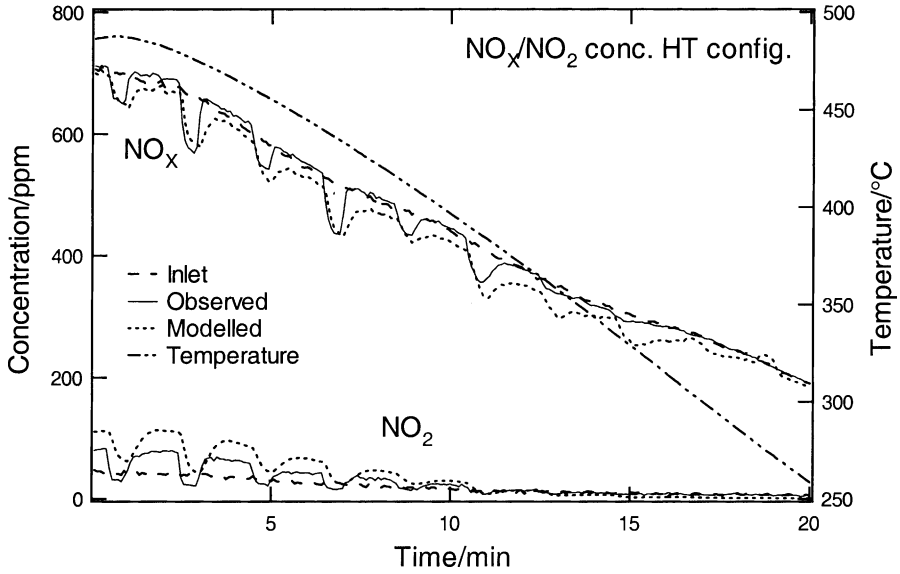

Fig. 8. Observed and modelled NO_x and NO_2 concentrations downstream the second HT catalyst during the temperature ramp with the HT configuration. Also shown are the temperature and the NO_x and NO_2 concentrations at the inlet to the first HT catalyst.

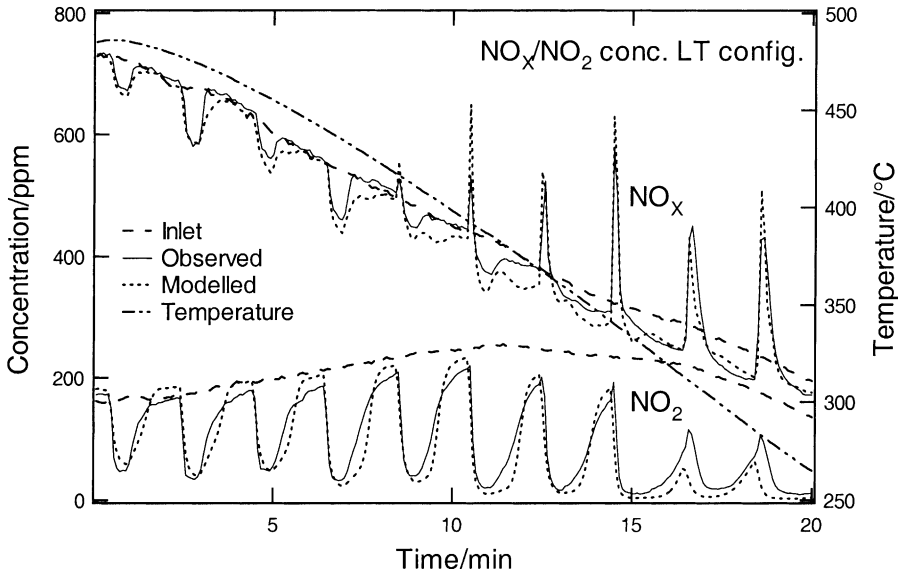

Fig. 9. Observed and modelled NO_x and NO_2 concentrations downstream the second HT catalyst during the temperature ramp with the LT configuration. Also shown are the temperature and the NO_x and NO_2 concentrations at the inlet to the first HT catalyst.

somewhat and instead the peak becomes broader. For the first two transients below 370 °C the NO_x concentration decreases to a value under the inlet concentration before the end of the hydrocarbon transient. The NO_x concentration then stays below the inlet concentration until the next hydrocarbon transient. For the following two transients the NO_x concentration decreases to a value under the inlet concentration after the end of the hydrocarbon transient. The integrated NO_x flow shows that there is a net conversion of NO_x for the three first transients below 370 °C. In the beginning of the transients the NO_2 concentration decreases fast and after the transient it increases slowly. Above 370 °C the NO_2 concentration almost reaches the inlet concentration before the next transient. Below 370 °C the NO_2 concentration increases more slowly as the temperature is decreased.

4. Discussion

Important parts of the catalyst model are the energy balances. The exhaust gas temperature varies widely and rapidly, causing temperature gradients along the catalyst. These gradients in turn affect the kinetics. For the kinetic model to be accurate the temperature of the catalyst also needs to be determined accurately. The thermal part of the catalyst model was validated with an ETC without injection. By using the LT configuration almost all engine out CO and hydrocarbon was converted in the LT catalyst before the exhaust gas reached the first HT catalyst. The HT catalyst could therefore be modelled with energy balances neglecting reaction heat. In Fig. 10, the observed and modelled temperature downstream the first HT catalyst during an ETC is shown. Also shown is the temperature at the inlet of the first HT catalyst.

The model is able to reproduce the heat exchange between the catalyst and the exhaust gas very well. There is no obvious phase difference between the modelled and the observed temperature, but the amplitude for some of the variations is smaller in the model than in the observations. The reason for this is probably the low number of tanks used in the model. The standard deviation is 3.9 °C.

The dynamic behaviour of the HT catalyst seems to be characterised by two different temperature regimes. Above 370 °C hydrocarbon conversion is high and there is a significant formation of CO. The response of CO to the transient hydrocarbon injection is immediate. Below 370 °C hydrocarbon conversion is considerably lower but still present. The CO response is slow in connection with both start and stop of hydrocarbon transients. This indicates that hydrocarbon is trapped on the surface and slowly converted to CO. The observation is in agreement with a previous study [4], where it was concluded that a hydrocarbon intermediate is formed.

Above 370 °C the NO_x conversion is related to the amount of added hydrocarbon and the NO_2 concentration does not have any notable influence on the NO_x conversion. Below 370 °C there is no obvious relation between the amount of added hydrocarbon and the NO_x conversion. An increased NO_2 concentration results both in an increased hydrocarbon conversion and in NO_x conversion at lower temperatures. It also results in a significant adsorption of NO_x that is released during hydrocarbon transients. The increased hydrocarbon and NO_x conversion at lower temperatures may be associated with the increased NO_x adsorption. Above 400 °C the increased NO_2 concentration results in higher hydrocarbon conversion whereas the NO_x conversion not is affected. At these temperatures no significant release of NO_x is observed during the hydrocarbon transients. A possible explanation

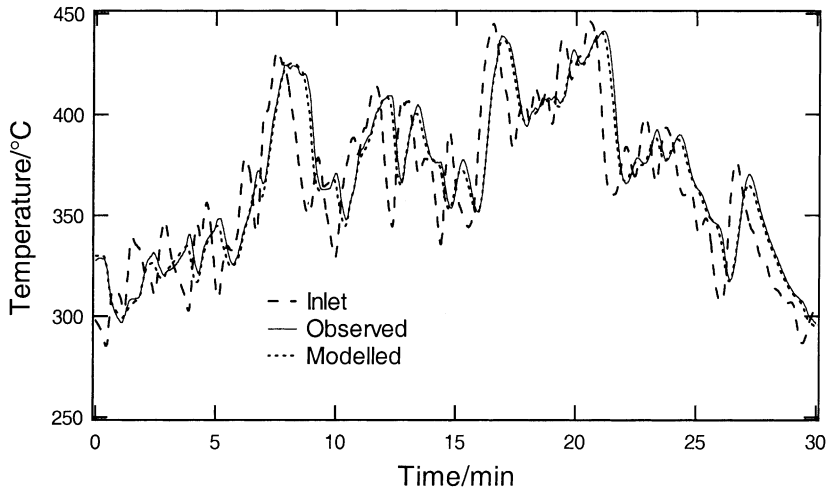

Fig. 10. Observed and modelled temperature downstream the first HT catalyst during an ETC. Also shown is the temperature at the inlet to the first HT catalyst.

for the increased hydrocarbon conversion could be that an increased NO_2 concentration keeps the surface more oxidised. NO_2 thus only influences the oxygen coverage but not the NO_x coverage and thereby not the NO_x conversion.

The hydrocarbon intermediate formed during hydrocarbon conversion cannot be directly related to the NO_x conversion, since the NO_x conversion below 370 °C then would be related to the amount of hydrocarbon added. It is, however, possible that another intermediate formed from the hydrocarbon intermediate is responsible for the NO_x conversion and that formation of the second intermediate is promoted by an increased NO_x coverage.

A number of intermediates have been detected or suggested on different catalysts during the reduction of NO_x by hydrocarbon. A partially oxidised hydrocarbon intermediate has been suggested to be associated with the reduction of NO_x by propene on Cu-ZSM-5 [15,16]. Also a N-containing intermediate has been proposed to be connected to the reduction of NO_x by propene on Cu-ZSM-5 [17] and by propane on Cu-ZrO_2 and Cu-ZSM-5 [18]. It has been shown that the reduction of NO_x by propane on HZSM-5 [19] and by propene on Cu-ZSM-5 [17] takes place more effectively with NO_2 than with NO. Furthermore, it has been suggested that the reduction of NO by propane on Pt/Al_2O_3 proceeds via the oxidation of NO to NO_2 on Pt, the adsorption of NO_2 on the Al_2O_3 support and the successive reaction between the adsorbed NO_2 and propane [20]. Surface nitrates have been detected on Ag/Al_2O_3 and have been shown to form isocyanate through the reaction with ethanol and methanol [21]. Surface nitrates have also been detected on Cu-ZSM-5 and have been shown to have a high reactivity with propane [22,23]. Isocyanate has been detected on the Al_2O_3 support and has been suggested to be an important intermediate during the reduction of NO by propene on Pt/Al_2O_3 [24,25]. Furthermore, isocyanate has been shown to react with NO and oxygen to form N_2 and N_2O on Pt/Al_2O_3 [26] and on Ag/Al_2O_3 [27].

Although the above mentioned catalysts have different activities, selectivity and temperature windows they have some common properties. NO_2 can under certain conditions promote NO_x reduction. Surface nitrates are formed which have high reactivity with hydrocarbons. N-containing intermediates, in some cases identified as isocyanates, are formed on the catalyst surface. These have for some catalysts been shown to react with NO to form N_2 and N_2O. In theory it is possible to describe all these catalysts with a general model that includes the least common set of surface species and the reactions they participate in. For each catalyst, the relative amount of different surface species and the rate of the different reactions they participate in then determine the dominating reaction pathways. Provided that the experimental data contain sufficient information, the fitting procedure will identify the significant reaction steps. From a modelling perspective, it is thus only required that a sufficient and suitable set of surface species and surface reactions is selected in order to obtain a successful model.

In recent works, Shimizu et al. have studied the selective catalytic reduction of NO by propene over Al_2O_3 [28] and Cu/Al_2O_3 [29]. With FT-IR spectroscopy surface nitrates and acetate were detected on both catalysts. Surface nitrates were formed at exposure to NO and oxygen and the rate of formation was higher on Cu/Al_2O_3 than on Al_2O_3. Acetate was formed in a flow of propene and oxygen and also in a flow of propene, NO and oxygen. The rate of acetate formation was higher in the flow of propene, NO and oxygen and the rate was higher on Cu/Al_2O_3 than on Al_2O_3. Acetate was also formed in a flow of propene only, after the catalyst had been exposed to a flow of NO and oxygen. The acetate reacted in flows of NO or oxygen alone or together and the reaction rate increased in the series NO $\ll$ oxygen $<$ NO and oxygen. N_2 formation was observed when NO and oxygen reacted with the acetate. On Cu/Al_2O_3 it was also observed that isocyanate and cyanide were formed when acetate reacted with NO and oxygen. The isocyanate was found to

react with NO alone or with NO and oxygen to produce N_2. The reaction rate was higher in the presence of both NO and oxygen.

The penetrating works by Shimizu et al. provide an almost complete reaction scheme for the reduction of NO_x by propene on Al_2O_3 and on Cu/Al_2O_3. Many of the features that are observed on these systems are also consistent with the properties of the HT catalyst. We therefore believe that the scheme provided by Shimizu et al. serves as a sound foundation for a feasible reaction mechanism for the HT catalyst. With support from the studies by Shimizu et al., the following reaction scheme was designed:

$$2S + O_2 \xrightarrow{r_1} 2S\text{–}O \quad (11)$$

$$2S\text{–}O \xrightarrow{r_2} 2S + O_2 \quad (12)$$

$$S + NO_2 \xrightarrow{r_3} S\text{–}NO_2 \quad (13)$$

$$S\text{–}NO_2 \xrightarrow{r_4} S + NO_2 \quad (14)$$

$$S\text{–}O + NO \xrightarrow{r_5} S\text{–}NO_2 \quad (15)$$

$$S\text{–}NO_2 \xrightarrow{r_6} S\text{–}O + NO \quad (16)$$

$$S\text{–}O + S\text{–}NO_2 \xrightarrow{r_7} S\text{–}NO_3 + S \quad (17)$$

$$S\text{–}NO_3 + S \xrightarrow{r_8} S\text{–}O + S\text{–}NO_2 \quad (18)$$

$$S\text{–}O + HC \xrightarrow{r_9} S\text{–}HC^* \quad (19)$$

$$2S\text{–}NO_3 + 3HC \xrightarrow{r_{10}} 2S\text{–}HC^* + CO + H_2O + 2NO \quad (20)$$

$$S\text{–}HC^* + S\text{–}O \xrightarrow{r_{11}} 2S + CO + H_2O \quad (21)$$

$$S\text{–}HC^* + S\text{–}NO_3 \xrightarrow{r_{12}} S\text{–}NO_2 + S + CO + H_2O \quad (22)$$

$$2S\text{–}HC^* + S\text{–}NO_3 \xrightarrow{r_{13}} 2S + S\text{–}NCO + CO_2 + 2H_2O \quad (23)$$

$$S\text{–}NCO + S\text{–}NO_3 \xrightarrow{r_{14}} 2S\text{–}O + CO_2 + N_2 \quad (24)$$

$$S\text{–}NCO + S\text{–}NO_2 \xrightarrow{r_{15}} 2S\text{–}O + CO + N_2 \quad (25)$$

$$S\text{–}O + CO \xrightarrow{r_{16}} S + CO_2 \quad (26)$$

$$S\text{–}NO_3 + CO \xrightarrow{r_{17}} S\text{–}NO_2 + CO_2 \quad (27)$$

S denotes an adsorption site. The rate expressions are given in Table 1. The kinetic model was fitted to experimental data both from the temperature ramp with the HT and the LT configuration and from the transient test. Fitting was first performed with the reaction between S–HC* and $S\text{–}NO_2$ to yield S–NCO and the reaction between S–NCO and S–O to yield NO and CO included in the reaction scheme. These reactions were found to be insignificant and were consequently removed from the reaction scheme. The number of sites (N_{cat}) was fitted to 0.324 ± 0.027 mol/kg catalyst (95% confidence). The values of the pre-exponential factors and the fitted activation energies together with 95% confidence intervals are given in Table 1. The confidence interval for the majority of the activation energies is less than 1 kJ/mol and the correlation (not shown in table) between most of the parameters is less than 0.9. This indicates that nearly all parameters are independently and well determined. The confidence interval is largest for the activation energy for reaction (24) (reaction between S–NCO and $S\text{–}NO_3$ to CO_2 and N_2). This indicates that this path for NO_x reduction is less significant than reaction (25) (where S–NCO reacts with $S\text{–}NO_2$), which is also reflected by the higher activation energy for reaction (14). The correlation is high (0.93) between the number of sites and the activation energy for reaction (19) (formation of S–HC* from S–O and HC). The high correlation is reasonable because this is an initial step that is not rate determining and it consequently results in a varying accumulation of S–HC* on the surface. Thus, both

Table 1
Rate expressions, pre-exponential factors and activation energies for the reactions on the HT catalyst point

Rate expression	Pre-exponential factor		Activation energy (kJ/mol)
$r_1 = k_1\theta_v^2$	2.13×10^5 m^3/(s kg catalyst)	Constraint	92.5 (±0.5)
$r_2 = k_2\theta_O^2$	3.24×10^{12} mol/(s kg catalyst)	Fixed	256.1 (constraint)
$r_3 = k_3 c_{NO_2}\theta_v$	1.78×10^5 m^3/(s kg catalyst)	Fixed	48.4 (±0.5)
$r_4 = k_4\theta_{NO_2}$	3.24×10^{12} mol/(s kg catalyst)	Fixed	111.8 (±0.7)
$r_5 = k_5 c_{NO}\theta_O$	7.33×10^4 m^3/(s kg catalyst)	Fixed	27.8 (±4.0)
$r_6 = k_6\theta_{NO_2}$	3.24×10^{12} mol/(s kg catalyst)	Fixed	67.4 (±4.3)
$r_7 = k_7\theta_O\theta_{NO_2}$	3.24×10^{12} mol/(s kg catalyst)	Fixed	84.7 (±2.4)
$r_8 = k_8\theta_{NO_3}\theta_v$	3.24×10^{12} mol/(s kg catalyst)	Fixed	124.5 (±2.0)
$r_9 = k_9 c_{HC}\theta_O$	8.05×10^4 m^3/(s kg catalyst)	Fixed	65.6 (±0.7)
$r_{10} = k_{10} c_{HC}\theta_{NO_3}$	8.05×10^4 m^3/(s kg catalyst)	Fixed	45.9 (±0.8)
$r_{11} = k_{11}\theta_{HC^*}\theta_O$	3.24×10^{12} mol/(s kg catalyst)	Fixed	177.1 (±0.9)
$r_{12} = k_{12}\theta_{HC^*}\theta_{NO_3}$	3.24×10^{12} mol/(s kg catalyst)	Fixed	133.9 (±0.8)
$r_{13} = k_{13}\theta_{HC^*}\theta_{NO_3}$	3.24×10^{12} mol/(s kg catalyst)	Fixed	139.4 (±0.9)
$r_{14} = k_{14}\theta_{NCO}\theta_{NO_3}$	3.24×10^{12} mol/(s kg catalyst)	Fixed	160.9 (±7.0)
$r_{15} = k_{15}\theta_{NCO}\theta_{NO_2}$	3.24×10^{12} mol/(s kg catalyst)	Fixed	99.0 (±0.7)
$r_{16} = k_{16} c_{CO}\theta_O$	2.28×10^5 m^3/(s kg catalyst)	Fixed	69.2 (±0.8)
$r_{17} = k_{17} c_{CO}\theta_{NO_3}$	2.28×10^5 m^3/(s kg catalyst)	Fixed	38.0 (±0.8)

The 95% confidence intervals are given for the fitted parameters; c_i and θ_i denotes the gas phase concentration and the surface coverage for species i; θ_v is equal to $1 - \sum\theta_i$; r_i and k_i denotes the reaction rate and the rate coefficient for reaction i.

the activation energy and the number of sites influence the coverage of this surface species. The correlation is also high (0.91) between the number of sites and the activation energy for reaction (26) (oxidation of CO with S–O). This is reasonable and indicates that the number of sites affects the oxygen coverage which in turn influences the reaction rate in a similar way as the activation energy. The correlation is furthermore, high (0.91) between the activation energies for reactions (22) and (23) (reaction between S–HC* and S–NO_3 to yield either S–NO_2 or S–NCO). This is reasonable since the difference in reaction rate for these two reactions depends entirely on the activation energies. The correlation is very high (0.999) between the activation energies for reactions (15) and (16) (oxidation of NO/reduction of NO_2). For these reactions the confidence intervals for the activation energies are also higher. Thus, it is rather the heat of reaction (the difference between the activation energies) than the individual activation energies that have been determined. This restricts the validity of the model to NO_x levels up to 1000 ppm (the upper level in the experiments used to fit the model). A simpler model with only S–NO_3 as adsorbed NO_x species did not generate high correlations. However, this model yielded a worse prediction of hydrocarbon and CO conversion. Experiments with synthetic exhaust gas may provide data for estimation of non-correlated parameters. However, one of the main purposes with this study is to develop a methodology for fitting models to data from experiments performed with real exhaust gas only.

In Figs. 11–13, the observed and the modelled concentrations of hydrocarbon, CO, NO_x and NO_2 downstream the first HT catalyst during the transient test are shown. Also shown are the concentrations of hydrocarbon, CO, NO_x and NO_2 at the inlet to the first HT catalyst. These results together with the results from the temperature ramp are discussed below.

At high temperatures, both in the temperature ramps (Figs. 4 and 5) and in the transient test (Fig. 11), the model overestimates hydrocarbon conversion. Furthermore, the sharp transition from high conversion above 370 °C to low conversion below this temperature, observed in the temperature ramps, is not well reproduced. One reason for this lack of fit may be that hydrocarbons are approximated as a single compound in the model, while diesel fuel in reality is a mixture of several hundred different hydrocarbons. Hydrocarbons in diesel fuel also differ from partially combusted hydrocarbons in exhaust gas, which probably explains deviations of observed and modelled hydrocarbon concentrations between the transients in the temperature ramp with the HT configuration. The shapes of many of the transients, especially tails following transients, are not well reproduced. The reason may be that the inlet hydrocarbon concentration not is sufficiently well described.

The model reproduces the CO concentration for the temperature ramp with the LT configuration reasonably well (Fig. 7). Above 370 °C the CO concentration is somewhat underestimated. The CO concentration is also underestimated during the entire temperature ramp with the HT configuration (Fig. 6). The CO concentration during the transient test is reproduced rather well (Fig. 12). The concentration is however underestimated for the large peaks around 30 min. The deviations for the CO concentration may to a large extent be associated with errors in the prediction of the hydrocarbon conversion as indicated above.

The model describes the concentration of NO_x and NO_2 reasonably well in the temperature ramp with both the HT (Fig. 8) and the LT (Fig. 9) configuration. In the LT

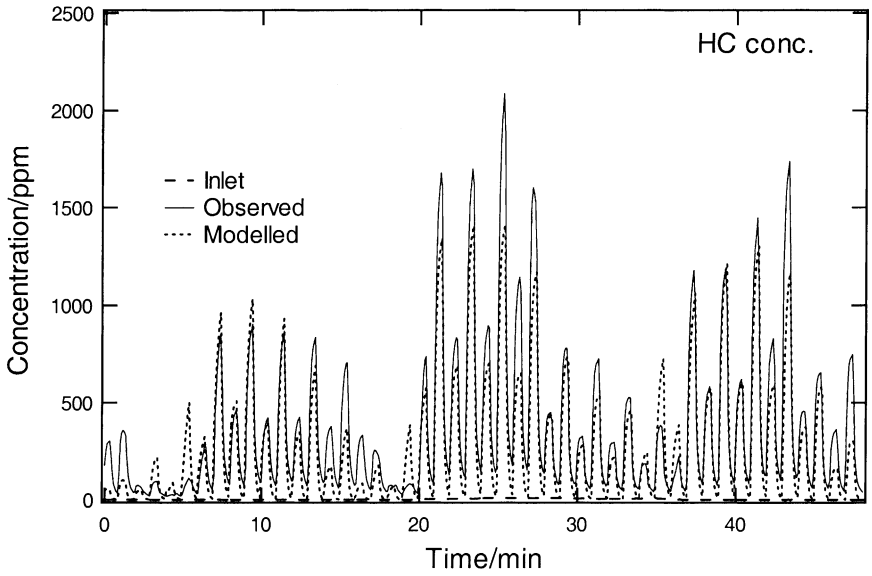

Fig. 11. Observed and modelled hydrocarbon concentrations (in C_1-units) downstream the first HT catalyst during the transient test. Also shown is the hydrocarbon concentration at the inlet to the first HT catalyst (injected hydrocarbon excluded).

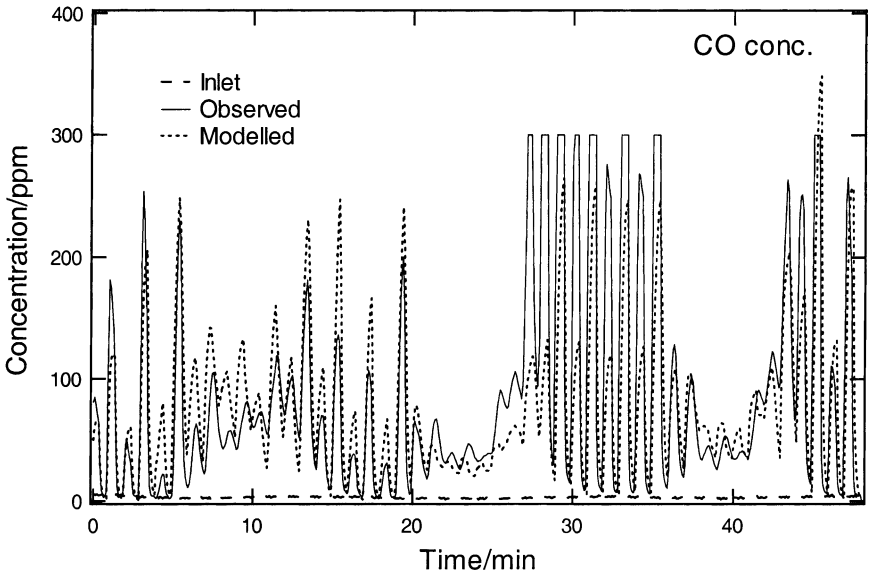

Fig. 12. Observed and modelled CO concentrations downstream the first HT catalyst during the transient test. Also shown is the CO concentration at the inlet to the first HT catalyst.

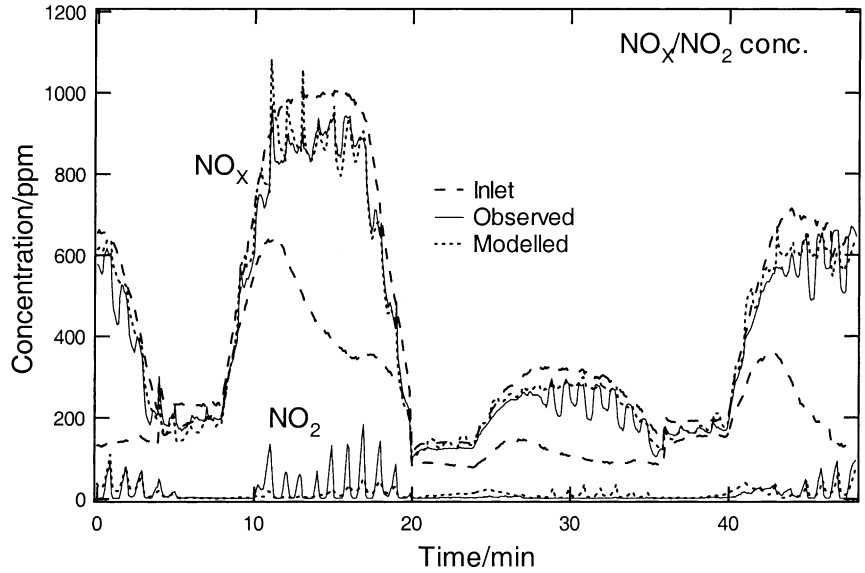

Fig. 13. Observed and modelled NO_x and NO_2 concentrations downstream the first HT catalyst during the transient test. Also shown are NO_x and NO_2 concentrations at the inlet to the first HT catalyst.

configuration the model is able to reproduce NO_x desorption peaks in the beginning of hydrocarbon transients, and also NO_x readsorption following hydrocarbon transients. NO_x conversion is however overestimated at low and intermediate temperatures. The agreement between observed and modelled NO_x and NO_2 concentration during the transient test is rather satisfactory (Fig. 13), although NO_x conversion is somewhat underestimated during the hydrocarbon transients around 3, 30 and 45 min. The NO_2 concentration is slightly underestimated between the hydrocarbon transients around 15 min and slightly overestimated between the hydrocarbon transients around 30 min. The reason for the overestimated NO_x conversion at low and intermediate temperatures is probably connected with the inability of the model to reproduce the sharp transition from low to high hydrocarbon conversion around 370 °C.

5. Conclusions

A systematic examination of a high temperature HC-SCR catalyst has been performed. Hydrocarbon conversion is high and the NO_x conversion is related to the amount of injected hydrocarbon above 370 °C. At lower temperatures

hydrocarbon conversion is low and NO_x conversion is not directly related to the injected hydrocarbon quantity. An increased inlet NO_2 concentration results in NO_x conversion at lower temperatures and also in accumulation of NO_x on the catalyst. Results are supported by recent findings by Shimizu et al. in studies of the selective catalytic reduction of NO by propene on Al_2O_3 and Cu/Al_2O_3. The present examination covers a major part of the operating range and is the foundation of a catalyst model constructed in agreement with conclusions of Shimizu et al. The model shows a reasonable consistency with experimental CO, NO_x and NO_2 data. Hydrocarbon conversion, however, is overestimated at high temperatures and the sharp transition from low to high conversion observed around 370 °C is not as well reproduced. A probable reason for the lack of fit, which to some extent affects also NO_x prediction performance, is that hydrocarbons are approximated as a single compound, whereas diesel fuel contains several hundred hydrocarbon species.

Acknowledgements

Thanks to Prof. Gunnar Lundholm for providing the engine rig, Johnson Matthey for providing the catalysts, Scania CV AB and Volvo Truck Corp. for their contributions to the project, Bengt Cyrén for assistance with the implementation of the rig control, Jan-Erik Everitt and Tom Hademark for practical assistance during tests. STEM, the Swedish National Energy Administration, is acknowledged for the financial support.

References

[1] S.L. Andersson, P.L.T. Gabrielsson, C.U.I. Odenbrand, AIChE J. 40 (1994) 1911.
[2] C. Künkel, C.U.I. Odenbrand, B. Westerberg, SAE Technical Paper 1999-01-3563, 1999.
[3] B. Westerberg, C. Künkel, C.U.I. Odenbrand, J. Chem. Eng. 87 (2002) 207.
[4] B. Westerberg, B. Andersson, C. Künkel, I. Odenbrand, Stud. Surf. Sci. Catal. 116 (1997) 317.
[5] K.C.C. Kharas, M.J. Miller, J.-I. Yan, SAE Technical Paper 982604, 1998.
[6] E.T. van der Laan, Chem. Eng. Sci. 7 (1958) 187.
[7] R.B. MacMullin, M. Weber Jr., Trans. AIChE 31 (1968) 409.
[8] R. Aris, Proc. R. Soc. A235 (1956) 67.
[9] E. Tronconi, P. Forzatti, AIChE J. 38 (1992) 201.
[10] R. Reid, The Properties of Gases and Liquids, 4th Edition, McGraw-Hill, New York, 1987, p. 515, p. 587, p. 597.
[11] I. Barin, Thermochemical Data of Pure Substances, Vols. 1/2, VCH, Weinheim, 1995.
[12] V.P. Zhdanov, Catal. Rev. Sci. Eng. 30 (1988) 501.
[13] J.A. Dumesic, D.F. Rudd, L.M. Aparicio, J.E. Rekoske, A.A. Treviño, The Microkinetics of Heterogeneous Catalysis, ACS, Washington, DC, 1993, pp. 26–40.
[14] J.R. Anderson, Structure of Metallic Catalysts, Academic Press, London, 1975, p. 296.
[15] C.J. Bennet, P.S. Bennet, S.E. Golunski, J.W. Hayes, A.P. Walker, Appl. Catal. A 86 (1992) L1.
[16] G.P. Ansell, A.F. Diwell, S.E. Golunski, J.W. Hayes, R.R. Rajaram, T.J. Truex, A.P. Walker, Appl. Catal. B 2 (1993) 81.
[17] M. Guyon, V. Le Chanu, P. Gilot, H. Kessler, G. Prado, Appl. Catal. B 8 (1996) 183.
[18] K.A. Bethke, C. Li, M.C. Kung, B. Yang, H.H. Kung, Catal. Lett. 31 (1995) 287.
[19] H. Hamada, Y. Kintaichi, M. Sasaki, T. Ito, M. Tabata, Appl. Catal. 70 (1991) L15.
[20] R. Burch, T.C. Watling, Stud. Surf. Sci. Catal. 116 (1998) 199.
[21] S. Kameoka, Y. Ukisu, T. Miyadera, Phys. Chem. Chem. Phys. 2 (2000) 367.
[22] T. Beutel, B.J. Adelman, G.-D. Lei, W.M.H. Sachtler, Catal. Lett. 32 (1995) 83.
[23] K. Hadjiivanov, D. Klissurski, G. Ramis, G. Busca, Appl. Catal. B 7 (1996) 251.
[24] F. Acke, B. Westerberg, L. Eriksson, S. Johansson, M. Skoglundh, E. Fridell, G. Smedler, Stud. Surf. Sci. Catal. 116 (1998) 285.
[25] D.K. Captain, M.D. Amiridis, J. Catal. 184 (1999) 377.
[26] F. Acke, B. Westerberg, M. Skoglundh, J. Catal. 179 (1998) 528.
[27] S. Sumiya, H. He, A. Abe, N. Takezawa, K. Yoshida, J. Chem. Soc., Faraday Trans. 94 (1998) 2217.
[28] K. Shimizu, H. Kawabata, A. Satsuma, T. Hattori, J. Phys. Chem. B 103 (1999) 5240.
[29] K. Shimizu, H. Kawabata, H. Maeshima, A. Satsuma, T. Hattori, J. Phys. Chem. B 104 (2000) 2885.